Biogeosciences, 9, 4885–4895, 2012
www.biogeosciences.net/9/4885/2012/
doi:10.5194/bg-9-4885-2012

Biogeosciences

Reconstructing skeletal fiber arrangement and growth mode in the coral *Porites lutea* (Cnidaria, Scleractinia): a confocal Raman microscopy study

M. Wall[1,2] **and G. Nehrke**[1]

[1]Alfred Wegener Institute for Polar and Marine Research, Am Handelshafen 12, 27570 Bremerhaven, Germany
[2]GEOMAR Helmholtz-Zentrum für Ozeanforschung Kiel, Wischhofstraße 1–3, 24148 Kiel, Germany

Correspondence to: M. Wall (mwall@geomar.de)

Received: 25 June 2012 – Published in Biogeosciences Discuss.: 10 July 2012
Revised: 2 November 2012 – Accepted: 9 November 2012 – Published: 28 November 2012

Abstract. Confocal Raman microscopy (CRM) mapping was used to investigate the microstructural arrangement and organic matrix distribution within the skeleton of the coral *Porites lutea*. Relative changes in the crystallographic orientation of crystals within the fibrous fan-system could be mapped, without the need to prepare thin sections, as required if this information is obtained by polarized light microscopy. Simultaneously, incremental growth lines can be visualized without the necessity of etching and hence alteration of sample surface. Using these methods two types of growth lines could be identified: one corresponds to the well-known incremental growth layers, whereas the second type of growth lines resemble denticle finger-like structures (most likely traces of former spines or skeletal surfaces). We hypothesize that these lines represent the outer skeletal surface before another growth cycle of elongation, infilling and thickening of skeletal areas continues. We show that CRM mapping with high spatial resolution can significantly improve our understanding of the micro-structural arrangement and growth patterns in coral skeletons.

1 Introduction

Scleractinian corals are marine organisms that thrive most vigorously in clear tropical oceans, forming one of the most important marine ecosystems – coral reefs. A thin layer of coral polyps secretes an aragonitic skeleton beneath their basal ectoderm forming an intricate and complex exoskeleton, which represents a chronologically layered archive. The fact that environmental information is recorded within these layered structures makes corals an important archive for palaeo-climate research. Even though coral reefs have been studied since Darwin's monography (Darwin, 1842) and successfully employed to learn about the past, the temporal relationship between microstructural elements is not fully understood. However, for high-resolution proxy analysis it is fundamental to deepen our understanding of biomineralization processes and growth pattern of corals.

The morphology of skeletal structures of corals represents the foundation of this investigation and will be explained in the following part, followed by a summary of the different biomineralization concepts that have been developed to explain their formation.

Each single polyp consists of different skeletal elements: a columella in the center, septa that radiate away from the center, a wall (theca and epitheca) and dissepiment bordering the corallite to the lateral and basal end, respectively (Milne-Edwards and Haime, 1857; Fig. 1). Adjacent corallites either share common walls or, if not, separated corallite walls are connected by skeletal elements forming the coenosteum. All of these macro-morphological elements can be more or less well developed depending on the coral genus (Sorauf, 1972; Veron, 2000; Nothurft and Webb, 2007). A close-up of a corallite, i.e. viewing individual macro-morphological skeletal elements (such as septa and columella), displays micro-morphological features such as spines, granules and nodules, which structure walls, septal margins and septal faces (Sorauf, 1972; Fig. 1a). The skeletons of the species studied in this investigation, *Porites lutea*, are relatively porous and less

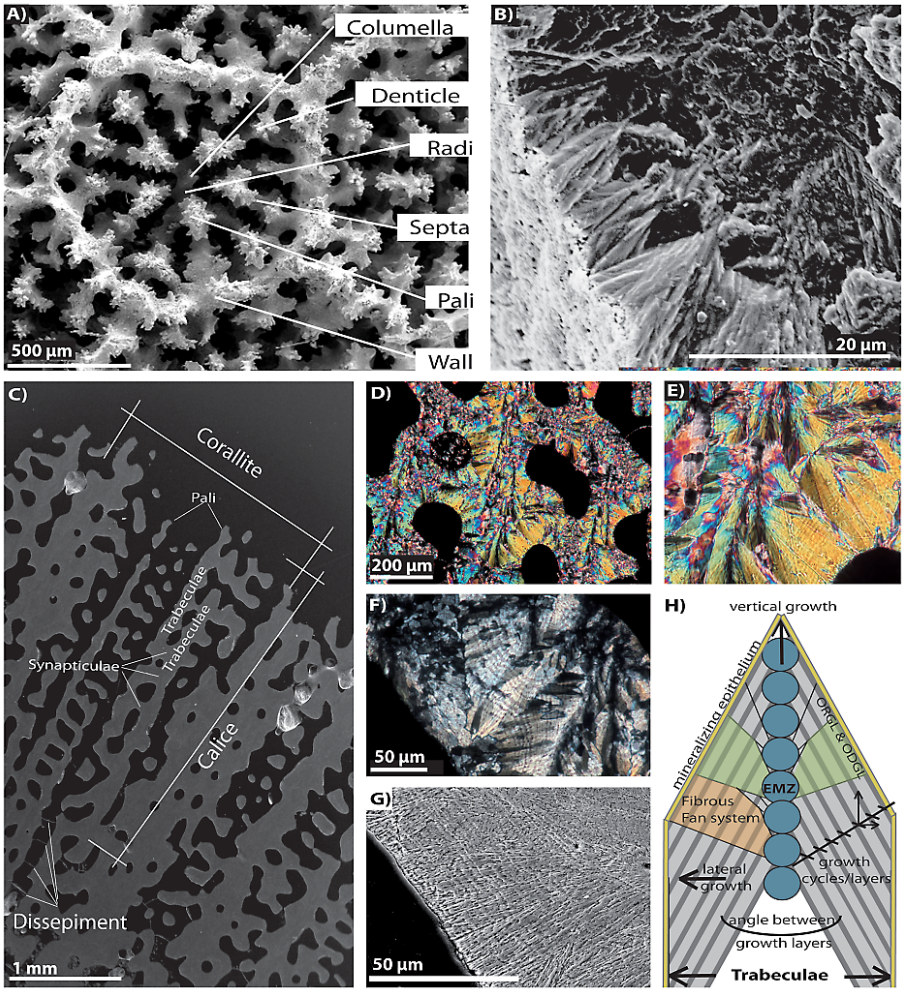

Fig. 1. Micrographs (SEM and PLM) and growth scheme of *P. lutea*. **(A)** SEM image of a corallite showing different macro-morphological elements. **(B)** Broken surface of septa showing the fibrous fan system. **(C)** Image of a longitudinal cross-section displaying skeletal elements forming the corallite. **(D)**–**(F)** Images taken by PLM show the fibrous fan system within the skeleton. Incremental growth layers are visible in the PLM images of the fibrous fan systems (**E** weakly visible growth layers in the lower right corner, **F** after ultrasonic alteration of sample surface). **(G)** Images of etched skeletal surfaces displaying the incremental nature of growth layers and the continuity of this layers between fibrous fan systems. **(H)** Schematic representation of coral skeletal growth of a trabeculae (modified after Cuif and Dauphin, 2005a). Stepping growth mode of fibrous fan-systems results in growth layers of organic-rich (ORGL, dark grey) and organic-depleted growth lines (ODGL, light grey) to both sides of the EMZ. The growth layers are oblique and encompass an angel resulting in differences in vertical and lateral extension per growth cycle.

differentiated into macro-morphological elements (Fig. 1) than other species (Sorauf, 1972; Barnes and Devereux, 1988; Nothurft and Webb, 2007). The skeleton is formed by vertical rods (trabeculae) that are interconnected horizontally by bars called synapticulae or radi, and each vertical rod terminates in pali or denticles (Fig. 1a and c) with several spines (Fig. 1a). Both macro- and micro-morphological elements are composed of two building blocks (microstructural elements): the centers of calcification (COC) and fibers. The COC – later described as early mineralization zone (EMZ) (Cuif et al., 2004) – build the scaffold for the coral skeleton ultimately responsible for the colony shape. They are arranged along the central axis and surrounded by fibers that represent the bulk of the skeleton (e.g. Cohen and McConnaughey, 2003; Nothdurft and Webb, 2007). These different skeletal morphological levels reflect the complex arrangement of coral skeletal elements and are specific for each taxon.

Early descriptive studies of coral skeletons focused on the classification of species but also led to the development of biomineralization concepts, of which the first date back to the end of the 19th century (e.g. Pratz, 1882; von Heider, 1886; von Koch, 1887; Oglivie, 1896). The first biomineralization concepts emphasize the resemblance of

microstructural elements as purely inorganic crystals. These growth concepts are based on a simple physico-chemical precipitation process, where centers act as "germs" and facilitate and direct the growth of aragonite crystals (Bryan and Hill, 1941; Barnes, 1970). Goreau (1959) observed a layer of organic compounds that he interpreted as a template for growth. Later scanning electron microscopy (SEM) revealed the incremental growth of coral fibers (Sorauf and Jell, 1977; Cuif and Dauphin, 1998). This insight, together with information from UV-fluorescence examinations, clearly demonstrated microstructural and chemical differences between fibers and centers of calcification (e.g. Cuif and Dauphin, 1998; Cuif et al., 1999). The incremental growth of coral fibers is expressed in the alternation of organic-rich and organic-depleted growth lines and a layered distribution of trace elements (Meibom et al., 2004, 2007) as well as sulphated polysaccharides. To explain the formation of these layered structures, Cuif and Dauphin (2005b) proposed a two-step mode of growth by introducing a sequential process acting at micrometer scale emphasizing an ectodermal control of biomineralization.

The recent coral growth concepts explain processes on the micrometer length scale such as growth of fibers around the EMZ. However, they do not provide a linkage to macroscopic structures such as synapticulae joining skeletal elements in regular intervals (Fig. 1c) or to temporal differences in formation of different skeletal elements and areas, such as secondary thickening of septa and the formation of dissepiments at the base of the polyp. A better understanding of coral growth patterns is desirable in order to improve the interpretation of high-resolution proxy data (Nothdurft and Webb, 2007). The high spatial resolution (sub-micrometer scale) of confocal Raman microscopy (CRM) has been demonstrated to be ideally suited to describe the structural relation between organic and inorganic phases in biogenic materials (e.g. Hild et al., 2008; Nehrke and Nouet, 2011; Neues et al., 2011; Nehrke et al., 2012). Recently, one study (Zhang et al., 2011) used CRM to map the skeleton of a blue coral (*Heliopora coerulea*, Octocorallia). They mapped a small region providing a preliminary insight into the ability of CRM to relate the distribution of organic compounds to the mineral phase in coral skeletons. In this study we applied CRM in combination with polarized light microscopy (PLM) and SEM to the scleractinian coral species *Porites lutea* (Milne-Edwards and Haime, 1860). The main focus was to describe the organic matrix distribution in relation to the mineral phase, in particular the organic-rich (ORGL) and organic-depleted (ODGL) growth lines (as first described in Cuif and Dauphin, 1998) that form a growth layer (the so-called environment recording unit as described by e.g. Cuif and Dauphin 2005a).

2 Material and methods

2.1 Coral sample

The scleractinian coral *P. lutea* was collected by scuba divers from an off-shore island in the Andaman Sea, Thailand, in March 2011. Coral tissue was removed by submerging the specimen in a 5 % sodium hypochlorite solution for 24 h, and subsequently rinsing with de-ionised water and drying for 24 h at 60 °C.

The flow chart in Fig. 2 provides an overview of samples derived from this specimen and gives an outline of the preparation and measurements applied. After tissue removal, three longitudinal and one transversal block were cut out of the skeleton and all but one of the longitudinal skeletal blocks were embedded in an epoxy resin (Araldite 2020, Huntsmann). All samples were ground using HERMES water grinding papers (in the order P1200, P2400, and P4000) and polished with a Struers diamond suspension of 3 µm and finished with a 0.3 µm aluminum oxide suspension. Each grinding and polishing step was followed by rinsing the sample with de-ionised water as well as a short cleaning using an ultrasonic bath. To determine how the observed structures continue into deeper levels of the skeleton, a vertical skeletal rod (trabeculae) of one sample was mapped by CRM in three different levels. This was done by re-grinding and polishing after each mapping to remove ~ 10 µm of the sample.

2.2 Confocal Raman microscopy

Raman spectroscopy is a method that allows determining many inorganic and organic compounds. It is based on light scattering of excited molecules. Most of the incident light is scattered elastically, which means that neither its kinetic energy nor its wavelength are changed, the so-called Rayleigh scattering. However, a very small fraction (1 out of 10^6–10^8) of photons are scattered inelastically and the re-emitted light is shifted in frequency. The inelastic scattering is due to excitation or annihilation of a molecular vibration. This results in a shift in energy that is characteristic for the molecule, and hence the obtained spectrum is a fingerprint of the analyzed sample (e.g. Smith and Dent, 2005; Dieing et al., 2011). The integration of a Raman spectrometer within a confocal microscope equipped with automated scanning stages makes it possible to map sample areas up to several mm^2. The use of continuously scanning high precision piezo stage enables to derive chemical images of samples even below diffraction limit (e.g. Dieing and Hollricher, 2008; Dieing et al., 2011). The datasets obtained during the scanning can contain up to a few hundred thousand spectra, from which the areal distribution of chemicals can be reconstructed. In mineral samples additionally crystallographic parameters such as crystallinity and crystal orientation can be constrained. Simultaneously, the biochemical composition can be mapped and related to the crystallographic observations. In this regard,

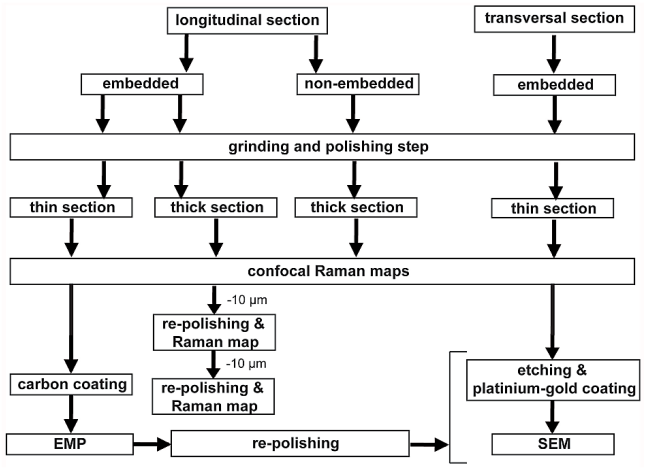

Fig. 2. Sample preparation and analysis overview. Flow chart displays the chronology of the preparation and measurement steps for samples.

CRM mapping/imaging represents an integrated and unique method to address the wide range of questions that are regularly raised in studies on biogenic structures.

In this study CRM mapping was done using a WITec alpha 300 R (WITec GmbH, Germany). Scans with a high spatial resolution were performed using a piezoelectric scanner table having a maximum scan range of 200 µm × 200 µm and a minimum step size of 4 nm lateral and 0.5 nm vertical. An ultra high throughput spectrometer (UHTS 300, WITec, Germany) equipped with an EMCCD camera was used with a grating of 600 grooves mm^{-1}, blazed at 500 nm. This set-up allows for a very short integration time (down to a few ms) and a spectral range from 0–3600 cm^{-1} or 0–4000 cm^{-1} depending on the wavelength used (532 nm or 488 nm, respectively). The Raman instrument was also operated as a normal light microscope using transmitted and reflected light and was equipped with a polarizing filter (one before the sample – the polarizer, and one after the sample – the analyzer). The analyzer can be used in the range from 500 to 800 nm allowing on the one hand the operation of the microscope for PLM and on the other hand for polarized Raman microscopy (at 532 nm). All Raman maps were obtained using a Nikon 100× (NA = 0.9) objective, with the polarizer set to 0° and the analyzer to 90°. The spectra during mapping were recorded with 0.5 µm spacing (for instance, for a 150 × 150 µm area, 300 × 300 data points/spectra were obtained) and an integration time of 50 ms or 10 ms for 532 or 488 nm, respectively. Raman measurements of biogenic materials are often hindered by strong fluorescence, which overlie distinct Raman lines. However, as shown by e.g. Nehrke and Nouet (2011) for the shell of the snail *Nerita undata*, fluorescence intensity distribution of a region can be used as a proxy to map organic matrix distribution within biogenic minerals. Thus, we used the spectral range between 2400–2700 cm^{-1} to map the fluorescence intensity distribution across the sample. The spectral analysis and data processing was performed using the WITec Project software (version 2.04, WITec GmbH, Germany).

2.3 Scanning electron microscopy

Prior to SEM analysis the samples were etched using 0.1 % formic acid and 3 % glutaraldehyde solution for 50 seconds to make microstructural features visible (Waite and Andersen, 1980; Cuif and Dauphin, 1998; Stolarski, 2003). After etching the sample was air-dried, put on aluminum stabs, and sputter-coated using a platinum/gold target. Scanning electron microscopic images were acquired at 10 kV or 15 kV and 1.7 µA filament current (Philips XL 30).

2.4 Electron microprobe mapping

Electron micro-probe mapping (EMP: JXA-8200 JEOL, GEOMAR) was used to study minor and trace element distribution in relation to the structures determined by CRM. The EMP maps were obtained by wavelength dispersive spectrometry (WDS) mode measuring simultaneously Mg (Ka, TAP), Sr (La, TAP) and S (Ka, PETH). The electron beam was focused to a spot size of 1 µm, accelerating voltage set to 15 kV and beam current to 20 nA. A step size of 1 µm as well as an accumulation time of 20 ms was used, and the map was repeated to gather 10 accumulations of the selected area. Standards (Vulcanicglass – VG-2) were measured before mapping the sample to calculate concentrations of the trace elements.

2.5 Growth layer thickness

Porites skeletons consist of vertical rods (trabeculae) that are built of EMZ and fibers (Fig. 1h). The fibers are deposited to both sides of the EMZ and composed of incremental growth layers (Cuif and Dauphin 2005a). The growth layer thickness was measured perpendicular to the outer coral mineralizing epithelium and comprises a pair of an ORGL and ODGL (see Fig. 1h). Both growth layer thickness and the angle between growth layers were measured in all Raman maps that displayed the alternation of ORGL and ODGL using the computer program ImageJ (Rasband, W. S., ImageJ, US National Institutes of Health, Bethesda, Maryland, USA, http://imagej.nih.gov/ij/, 1997–2012).

3 Results and discussion

3.1 Structural sample characterization

The spectroscopic datasets obtained during the different Raman mappings were first analyzed for the characteristic Raman peaks of aragonite (Fig. 3): translational mode (155 cm^{-1}), librational mode (208 cm^{-1}), in-plane bend

($710\,cm^{-1}$) and symmetric stretch ($1085\,cm^{-1}$) (Bischoff et al., 1985; Urmos et al., 1991). The differences in crystallographic orientation of aragonite fibers (Fig. 3c) were visualized by using the relative peak intensity changes as shown by Nehrke and Nouet (2011) for the orientation of aragonite prisms in a gastropod shell. The CRM images (Fig. 3b) show the typical fan-like fibers (Pratz, 1882; Oglivie, 1896) for scleractinian coral skeletons using PLM (Fig. 3c). The relative intensity distribution of the major aragonite peak at $1085\,cm^{-1}$ can be used to visualize changes in crystal orientations. The visualization of these orientations was possible in embedded as well as non-embedded polished samples. Hence, structural information of the mineral phase and relative orientation can be derived without preparation of thin section, as required for PLM.

Simultaneously, the fluorescence intensity maps provide the distribution and arrangement of the organic matrix within coral skeletons. Both the distribution of incremental ORGL and the EMZ (e.g. Cuif and Dauphin, 1998) could be visualized (Figs. 4 and 5) as revealed by former studies by the means of acridine orange staining (Cuif and Dauphin, 1998; Cuif et al., 1999; Gautret et al., 2000; Stolarski, 2003). The distribution of the organic matrix mapped by CRM can directly be compared to the structures visualized in SEM micrographs of the etched sample (Fig. 5). The superimposed maps of crystal orientation and fluorescence (Fig. 4) confirmed the synchronism in formation of growth layers between adjacent fibers (Cuif et al., 2004) and their relative orientation with respect to the major growth limit. Therefore, Raman mapping can simultaneously determine differences in crystallographic orientation, the distribution of incremental growth layers, and the location of the EMZ within corals without applying acridine orange staining or etching of the sample surface. This improves the interpretation of data while reducing the number of different sample preparation steps and therewith the possibility of sample alteration (which allows to perform additional analytical investigations on the same sample).

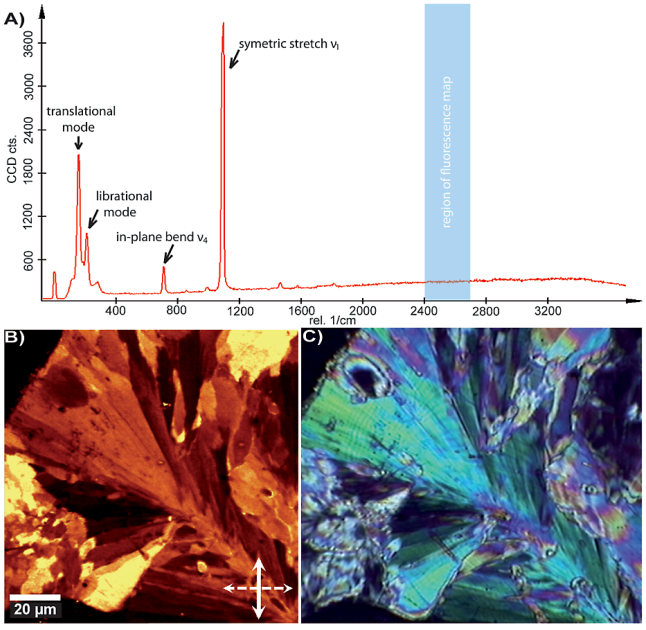

Fig. 3. Raman spectra, Raman intensity map and PLM image illustrating the crystallographic orientation within the fan system. **(A)** Raman spectra of *P. lutea* skeleton sample showing the characteristic peaks for aragonite. Highlighted in blue is the spectral region used to derive the fluorescence maps. **(B)** Relative change in crystallographic orientation derived from the Raman peak at $1085\,cm^{-1}$ resembles the fiber orientation shown in the PLM image **(C)**. Solid arrow in **(B)** indicates the laser polarization plane and dashed arrow the orientation of the analyzer.

3.2 Growth layers

Based on the previously described results, fluorescence images can be used to derive information on growth layer thickness. The distances of growth layers were measured perpendicular to the growth lines and equal to a distance of 3.9 ± 0.2 µm (mean $\pm$SE; $n = 18$). These layers encompass on average an angle of $36 \pm 2°$ (mean $\pm$SE; $n = 16$), and hence a growth layer results in a mean vertical extension of 12 µm (calculation: growth layer thickness/sin; angle between growth layers/2). This vertical extension was compared to the mean daily growth rate of this specimen of approx. $30\,\mu m\,day^{-1}$ (derived from staining of the specimen 3 months prior to collection). Even though the assumption of linear growth does not account for the cyclicity of the growth processes, it provides an estimate of how much the corals in average extents per day and allows to compare daily growth cycle numbers from the literature. These data suggest that per day 2–3 growth cycles occur. Meibom et al. (2007) compared average linear extension rates to distances between high Mg bands determined by means of NanoSIMS measurements (on *Porites* sp.) and suggested that within a day up to five growth cycles could be deposited. In his measurements, one growth layer was between 2–5 µm wide. Thus, both cyclicity and growth layer thickness correspond to the values obtained in this study and support the capability of CRM to trace growth lines. Cuif et al. (2011) obtained 10–15 cycles per week ($\sim$ 2 cycles per day) for *Galaxea fascicularis* from a consecutive calcein staining experiment. Thus, this study and the study by Meibom et al. (2007) observed a slightly higher number of cycles per day for *Porites* spp. than Cuif et al. (2011) for *Galaxea fascicularis*. Nothdurft and Webb (2007) observed that a vertical extension of 384 µm equals 36 µm in lateral growth by tracking growth lines in a skeletal rod of *Porites lobata*. This vertical distance was deposited within 12 days (derived from mean growth rates for this species; see Nothdurft and Webb, 2007) and equals a lateral growth of 3 µm per day. Based on the growth rates determined in this study and the study by Meibom et

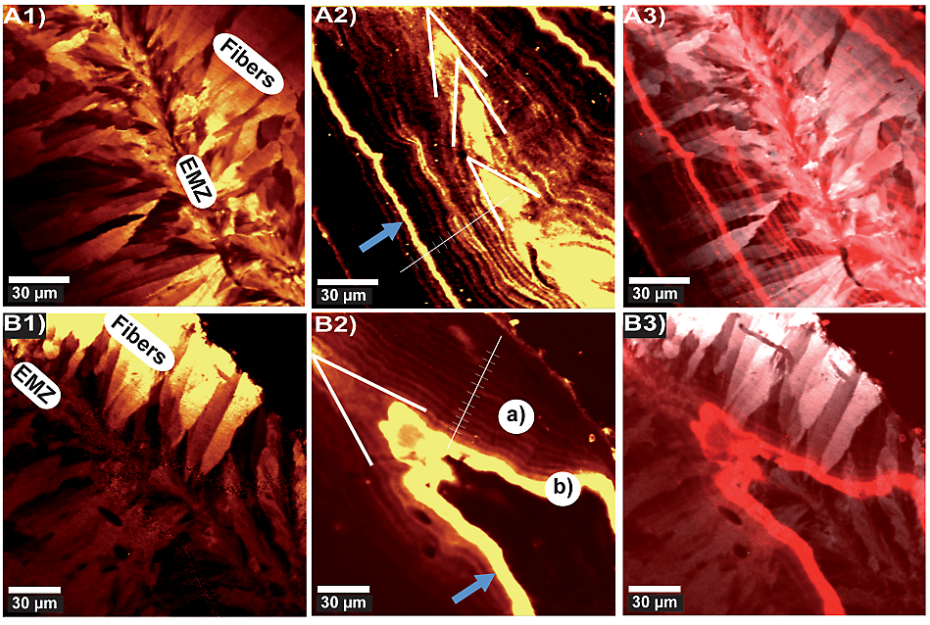

Fig. 4. Raman maps obtained on longitudinal thin sections (**A** and **B**) of the skeleton of *P. lutea*. Numbers indicate the spectral region used for the maps: **(1)** represents the intensity distribution of the symmetric stretch of aragonite (1085 cm^{-1}); **(2)** the fluorescence intensity distribution; and **(3)** shows the superposition of map **(1)** and **(2)**. Blue arrows indicate organic-rich growth lines (ORGL 2) showing increased fluorescence within fluorescence maps. White arrowheads represent the oblique traces of the position of mineralizing epithelium forming layered growth increments with a high and a low fluorescence growth line comprising one growth cycle. The scale bar within fluorescence maps displays the skeletal extension for each growth cycle. The two types of growth lines within fluorescence maps are indicated in **(B2)** with **(a)** representing the incremental growth layers (organic-rich and organic-depleted growth lines) and **(b)** the high fluorescence growth lines (ORGL 2). (Superimposed images derived from WITec Project software.)

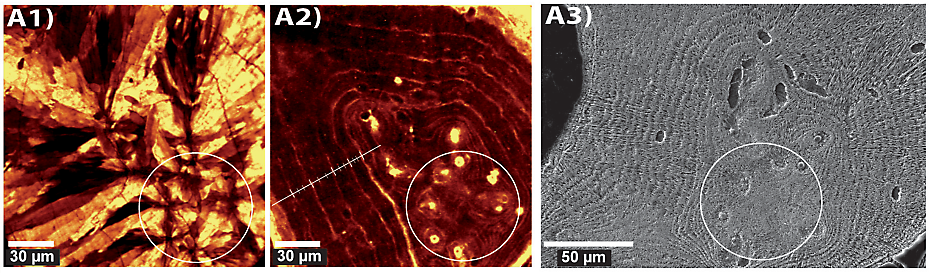

Fig. 5. Transversal cross section of the skeleton of *P. lutea*. Map obtained from the Raman intensity distribution of the symmetric stretch of aragonite (1085 cm^{-1}), **(A1)** and fluorescence intensity distribution **(A2)**. **(A3)** A SEM micrograph obtained after Raman mapping and etching of the sample. Circle in the images illustrates the same area within the different maps. The scale bar within the fluorescence map displays the skeletal extension for each growth cycle comprised of one high and one low fluorescence growth line.

al. (2007), 3 µm lateral growth corresponds to approximately one growth cycle per day.

The differences in growth cycles per day could have various nature and are suggested to derive from (1) stress from the staining process (Thebault et al., 2006; Houlbreque et al., 2009), (2) nutritional status (Cuif et al., 2011), (3) species-specific differences (Cuif et al., 2011), and/or (4) growth rates could differ depending on the location within the skeleton. All of these factors may be relevant; however, a nonlinear growth rate in lateral and longitudinal direction, different growth rates depending on the distance from the EMZ and non-regular growth can explain the observed decrease in number of growth cycles when tracing growth lines over larger areas. This assumption is also supported by the observed arrangement of growth lines – reflecting a non-regular growth – determined by CRM mapping (Fig. 6a and b) and SEM images (Nothdurft and Webb, 2007).

In this study we detected two types of ORGL, showing significant differences in thickness and intensity within the CRM maps. From here on the wide growth lines showing

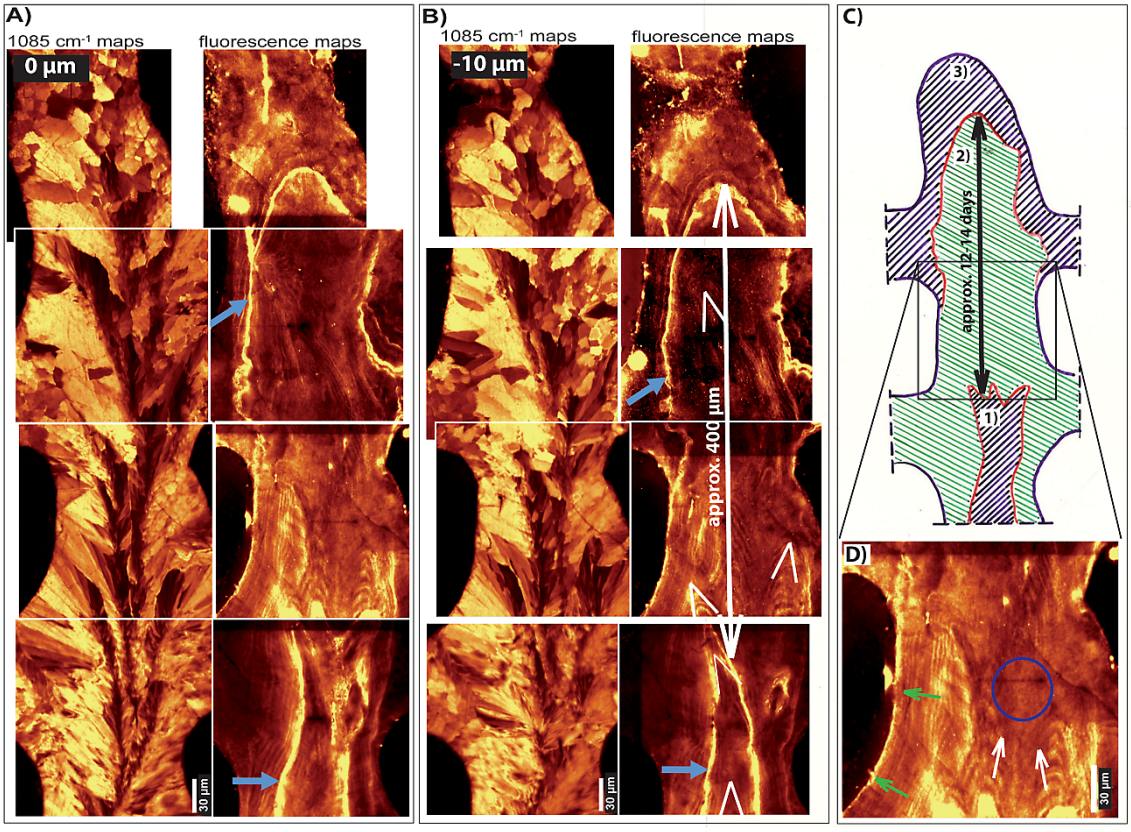

Fig. 6. (**A** and **B**) Raman maps in different depth levels (**A**: 0 µm, **B**:−10 µm) of intensity distribution of the symmetric stretch of aragonite and of fluorescence are plotted on the left and right, respectively. Blue arrows indicate repeated features of organic-rich growth lines (ORGL 2) of increased fluorescence detected within fluorescence maps. White arrowheads represent the oblique traces of the position of mineralizing epithelium forming layered growth increments with a high and a low fluorescence growth line comprising one growth cycle. The scale bar within fluorescence maps displays the skeletal extension for each growth cycle. (**C** and **D**) Schematic representation of growth patterns mapped with confocal Raman microscopy. **(C)** Schematic image of cyclicity in growth representing three cycles each ending with a high fluorescence growth line (red line), which equals approx. 12–14 day periodicity (daily growth rate of this specimen of $\sim 30\,\mu m\,d^{-1}$). **(D)** During each cycle different growth modes are suggested to be responsible for the three-dimensional appearance of the skeletal vertical rod. Vertical extension in the direction of the spines reflects thicker growth layers (white arrows) than in lateral growth. Lateral growth represents thickening of skeletal element (green arrows) and both lateral and vertical growth potentially is associated with different growth rates. Blue circle marks an area of a not clearly visible banding pattern where the skeleton was potentially sectioned parallel to the position of the growth layers.

increased fluorescence (indicated by a blue arrow within Raman fluorescence maps; Figs. 4 and 6) are referred to as ORGL 2 (Fig. 4B2 b) whereas the thinner incremental growth lines are referred to as ORGL 1 (Fig. 4B2 a).

3.3 Growth patterns and cyclicity

The temporal heterogeneity in skeletal formation also becomes obvious when trying to track spines along the corallite into deeper parts of the skeleton, where it appears that they are not present. Hence, different regulative processes must act to produce the spine-rich distal end of the corallites, the skeletal layer covering spines above dissepiments before the skeleton is cut off from the polyp as well as the formation of synapticulae at a regular interval. It could be shown that the ORGL 2 continue in deeper skeletal layers of a vertical rod (Fig. 6a and b). Moreover, these lines resemble the coral outer surface forming a three-dimensional organic envelope. We hypothesize that these ORGL 2 act as an "envelope" representing the outer surface at a certain time of deposition (Fig. 6c), before it becomes overgrown and covered by a next growth cycle. The temporal units 1 to 3 in Fig. 6c represent different growth cycles with 1 being the oldest and 3 the youngest deposited skeleton. Each growth cycle lasts about two weeks and ends with an ORGL 2 (Fig. 6c). Within this biweekly cycle elongation, infilling between spine tips and thickening of macro-morphological elements takes place (Fig. 6d). This periodicity in growth agrees with the growth model proposed by Nothdurft and Webb (2007). They traced a growth band in their study (Nothdurft and Webb, 2007;

their figures 16c and 17b) that resembles the ORGL 2 described in this study (Fig. 6) with a similar longitudinal extension spanning approx. 12 days of growth. This observation supports the proposed mechanism of a three-dimensional structural regulation by ORGL 2 in *Porites* skeletal growth that follows a biweekly periodicity.

Cyclicity represents a ubiquitous characteristic of coral skeletal formation. The described cycles range from the cm-level displayed by seasonal density bands (e.g. Lough and Barnes, 2000) down to the µm-level of daily/sub-daily formation of incremental growth layers (e.g. Meibom et al., 2007). High-resolution proxy studies detected a cyclicity of measured proxy values in the range of weekly to monthly periods (Meibom et al., 2003; Rollion-Bard et al., 2003; Cohen and Sohn, 2004; Allison et al., 2010, 2011). In these studies the proxy relation (e.g. Sr / Ca) did not only depend on the target parameter (e.g. T) but was potentially influenced by other parameters like (1) metabolic changes involving spawning and larval release at a lunar periodicity (Meibom et al., 2003), (2) weekly tidal forcing overlying temperature forcing (Cohen and Sohn, 2004), and (3) a strong bi-weekly periodicity that was hypothesized to result from increased calcification required for the formation of synapticulae (Cohen and Sohn, 2004). The latter corresponds to the biweekly growth bands (ORGL 2) described in this study.

3.4 Possible contributions of CRM to biomineralisation research – an outlook

3.4.1 Chemical characterization of organic compounds

So far we have used the intensity of the fluorescence determined by CRM as a "black box" for organic molecules. This concept is sufficient since the scope of this investigation is on structural information of coral skeletons in relation to three-dimensional growth patterns and not the characterization of organic compounds. The emphasis was laid on obtaining Raman maps of high spatial resolution (requiring a hundred thousand spectra per scan) for structural analysis. However, it should be pointed out that CRM is much more powerful and can deliver more detailed information for the chemical characterization. To demonstrate what kind of chemical information can be obtained, we analyzed the spectra of some areas showing increased fluorescence in more detail (longer integration time) and compared the spectra to other studies using Raman spectroscopy on biominerals. Spectral lines not attributed to aragonite were detected (Fig. 7) corresponding to asymmetric SO_4^{2-} bend (646 cm^{-1}, Jolivet et al., 2008; Zhang et al., 2011), Amid III (1190–1310 cm^{-1}, Jolivet et al., 2008; Zhang et al., 2011), CH bands (2850–3080 cm^{-1}, Perrin and Smith, 2007; Jolivet et al., 2008) and OH-groups (3200–3400 cm^{-1}, Jolivet et al., 2008). Recent studies used Raman spectroscopy to characterize organic matrix in biominerals (Kaczorowska et al., 2003; Perrin and Smith, 2007; Jolivet et al., 2008; Zhang et al., 2011; Nehrke and Nouet, 2011;), but coral Raman spectroscopic analyses covering a spectral region between 100–3200 cm^{-1} are quite rare. However, these studies already demonstrated the ability to observe differences in quantity (not absolute but relative Figs. 4–7, this study and Perrin and Smith, 2007 for corals; Jolivet et al., 2008, for otoliths; Nehrke and Nouet, 2011, for molluscs) and quality (Fig. 7, also Perrin and Smith, 2007) by Raman spectroscopy/microscopy within samples. Zhang et al. (2011) even discussed the potential to retrieve diurnal environmental variability of phosphorus by mapping the intensity distribution of the symmetric P-O stretch. Corals are well known

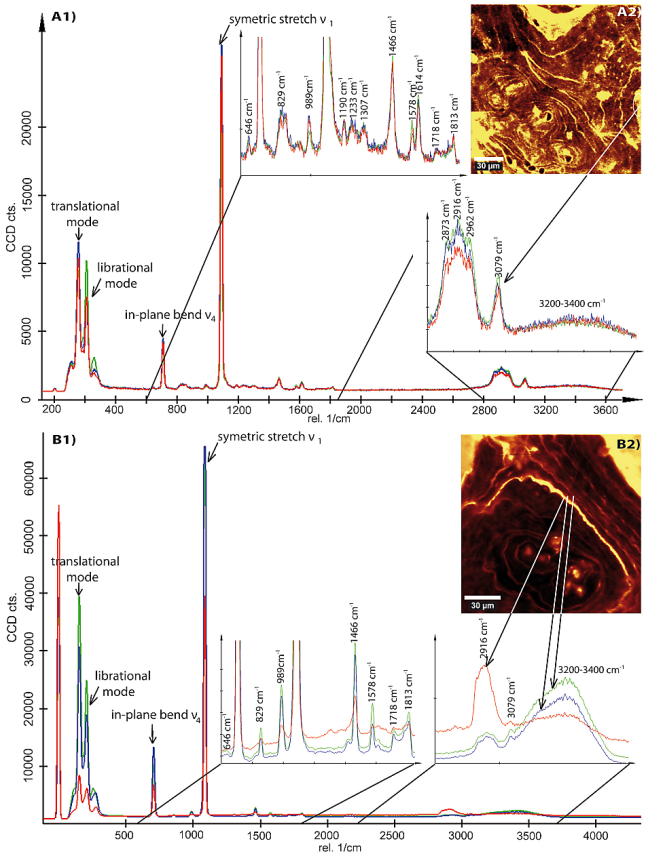

Fig. 7. Raman spectra obtained on a skeleton sample of *P. lutea* showing the characteristic peaks for aragonite (translational mode at 155 cm^{-1}, librational mode at 208 cm^{-1}, in-plane band at 710 cm^{-1} and symmetric stretch at 1085 cm^{-1}). Regions of minor peaks are zoomed out: 600–1850 cm^{-1} and 2800–3600 cm^{-1}. Raman spectra using longer integration times were obtained after mapping the region marked in the fluorescence map in **(A2)** and **(B2)** with following settings for **(A1)**: 532 nm laser wavelength, centered at 2000 cm^{-1}, integration time of 0.5 s and 10 accumulations, 100× Nikon objective, analyzer set 90°to laser wavelength and **(B1)**: 488 nm laser wavelength, centered at 2400 cm^{-1}, integration time of 6 s and 10 accumulations, 100× Nikon objective. (Raman spectra were derived in different points and displayed by different colours.)

for recording environmental parameters, but high-resolution analysis revealed some constraints associated with the skeletal structural complexity (e.g. Meibom et al., 2004; Cuif and Dauphin, 2005b; Juillet-Leclerc et al., 2009; Rollion-Bard et al., 2010). The wealth of chemical information obtained by CRM can potentially be applied to acquire environmental information and complement proxy studies. However, this can only be achieved by better understanding the process of biomineralization. Structural analyses of coral skeletons by CRM can contribute to better understand coral growth patterns and potentially help to interpret heterogeneities observed in high-resolution proxy analyses. Additionally, characterization of chemical compounds and their spatial distribution can deliver new insight into chemical compounds involved in calcification.

3.4.2 Correlation between organic matrices and elemental composition

We performed EMP mapping on the same sample previously investigated by CRM to demonstrate how information on the element distribution and those obtained by CRM can be related to each other. The results qualitatively agree with previous studies (Cuif et al., 2003; Meibom et al., 2004, 2007, 2008), even though the resolution of EMP is not comparable with high-resolution techniques like XANES or NanoSIMS (Cuif et al., 2003; Meibom et al., 2004). For example, a cyclic variation of S within fibers could not be resolved in this study. Preliminary results indicate that the two types of ORGL differ in Mg concentration with the ORGL 1 showing elevated Mg concentrations in contrast to ORGL 2. In general it is assumed that in corals Mg is associated with organic compounds (Finch and Allison, 2008), which often also show increased S concentrations (Cuif et al., 2012). However, the ORGL 2 do not follow this pattern but show decreased Mg concentration and no increase in S. The low Mg in ORGL 2 most likely corresponds to the distinct low Mg lines described by Meibom et al. (2004, their figure 2 – *Pavona clavus*; 2007, their figure 2 – *Porites* sp.). Therefore, these lines would represent a structural feature not restricted to the skeleton of *P. lutea*.

4 Conclusions

In the present study we used CRM on *P. lutea* skeleton samples to demonstrate

1. that mapping by CRM can be used to visualize relative differences in crystal orientation, without the necessity to prepare thin sections, as required if this information is obtained by PLM;

2. that the position of the EMZ and the layered distribution of organic-rich growth lines can be visualized and related to the orientation of fibers;

3. that two different types of organic-rich growth lines are present. One of these growth lines corresponds to the well-known incremental growth lines. In contrast, the second type of organic-rich growth lines (within the text referred to as ORGL 2) resembles denticle finger-like structures (traces of former spines or previous skeletal surfaces). Preliminary results indicate that the latter is characterized by a lower Mg concentration;

4. that CRM mapping can provide information on skeletal growth patterns by tracking growth lines within a skeletal rod not only in two dimensions but also in in depth;

5. and that Raman spectra of organic compounds can be measured. The latter represents a powerful possibility in the chemical characterization of organic compounds within coral skeletons.

Simultaneously obtained information on structural and chemical information can deepen our understanding of growth pattern in coral skeletons and improve growth concepts above the micrometer scale. Organic compounds are hypothesized to play a crucial role in coral biomineralisation. Analytical methods like e.g. nanoSIMS, or XANES are crucial in the investigation of biogenic materials but are restricted by the small area that can be investigated. Thus, the possibility to apply these methods to the same area previously characterized by CRM is highly valuable, as demonstrated by the preliminary EMP measurements, which revealed the presence of chemically different growth lines in *P. lutea*.

Acknowledgements. The authors would like to thank J.-P. Cuif and one anonymous reviewer for their helpful and constructive comments, which helped to improve the manuscript. We thank Jan Fietzke (GEOMAR) for the assistance with the EMP measurements. This work was supported by the European Commission through grant 211384 (EU FP7 “EPOCA”), the German Federal Ministry of Education and Research (BMBF, FKZ 03F0608, “BIOACID”), the European Community’s Seventh Framework Programme (FP7) under grant agreement 265103 (Project MedSeA) and has received funding from the FP7-PEOPLE-2007-1-1-ITN Marie Curie Action: CalMarO (Calcification by Marine Organisms, Grant number: 215157).

Edited by: J. Toporski

References

Allison, N., Finch, A. A., and EIMF: The potential origins and palaeoenvironmental implications of high temporal resolution δ18O heterogeneity in coral skeletons, Geochim. Cosmochim. Ac., 74, 5537–5548, doi:10.1016/j.gca.2010.06.032, 2010.

Allison, N., Cohen, I., Finch, A. A., Erez, J., and EIMF: Controls on Sr/Ca and Mg/Ca in scleractinian corals: The effects of Ca-ATPase and transcellular Ca channels on

skeletal chemistry, Geochim. Cosmochim. Ac., 75, 6350–6360, doi:10.1016/j.gca.2011.08.012, 2011.

Barnes, D. J.: Coral skeletons: an explanation of their growth and structure, Science, 170, 1305–1308, 1970.

Barnes, D. J. and Devereux, M. J.: Variations in skeletal architecture associated with density banding in the hard coral *Porites*, J. Exp. Mar. Biol. Ecol., 121, 37–54, doi:10.1016/0022-0981(88)90022-6, 1988.

Bischoff, W. D., Sharma, S. K., and Mackenzie, F. T.: Carbonate ion disorder in synthetic and biogenic magnesian calcites: a Raman spectral study, Am. Mineral., 70, 581–589, 1985.

Bryan, W. and Hill, D.: Spherulitic crystallization as a mechanism of skeletal growth in the hexacorals, Proc. R. Soc. Queensl., 52, 78–91, 1941.

Cohen, A. L. and McConnaughey, T.: Geochemical perspectives on coral mineralization, in: Biomineralization, edited by: Dove, P. M., Weiner, S., and de Yoreo, J. J., Reviews in Mineralogy and Geochemistry, Mineralogical Society of America, 2003.

Cohen, A. L. and Sohn, R. A.: Tidal modulation of Sr/Ca ratios in a Pacific reef coral, Geophys. Res. Lett., 31, L16310, doi:10.1029/2004gl020600, 2004.

Cuif, J.-P. and Dauphin, Y.: Microstructural and physico-chemical characterization of "centers of calcification" in septa of some recent scleractinian corals, Palaeontol. Z., 72, 257–270, 1998.

Cuif, J. P. and Dauphin, Y.: The Environment Recording Unit in coral skeletons – a synthesis of structural and chemical evidences for a biochemically driven, stepping-growth process in fibres, Biogeosciences, 2, 61–73, doi:10.5194/bg-2-61-2005, 2005a.

Cuif, J.-P. and Dauphin, Y.: The two-step mode of growth in the scleractinian coral skeletons from the micrometer to the overall scale, J. Strut. Biol., 150, 319–331, 2005b.

Cuif, J. P., Dauphin, Y., and Gautret, P.: Compositional diversity of soluble mineralizing matrices in some recent coral skeletons compared to fine-scale growth structures of fibres: Discussion of consequences for biomineralization and diagenesis, Int. J. Earth Sci., 88, 582–592, doi:10.1007/s005310050286, 1999.

Cuif, J.-P., Dauphin, Y., Doucet, J., Salomé, M., and Susini, J.: XANES mapping of organic sulfate in three scleractinian coral skeletons, Geochim. Cosmochim. Ac., 67, 75–83, 2003.

Cuif, J.-P., Dauphin, Y., Berthet, P., and Jegoudez, J.: Associated water and organic compounds in coral skeletons: quantitative thermogravimetry coupled to infrared absorption spectrometry, Geochem. Geophy. Geosy., 5, doi:10.1029/2004GC000783, 2004.

Cuif, J.-P., Dauphin, Y., and Sorauf, J.: Biominerals and fossils through time, Cambridge University Press, Cambridge, 490 pp., 2011.

Cuif, J.-P., Dauphin, Y., Nehrke, G., Nouet, J., and Perez-Huerta, A.: Layered growth and crystallization in calcareous biominerals: Impact of structural and chemical evidences on two major concepts in invertebrate biomineralization studies, Minerals, 2, 11–39, 2012.

Darwin, C.: The structure and distribution of coral reesf, University of California Press, London, UK, 1842.

Dieing, T. and Hollricher, O.: High-resolution, high-speed confocal raman imaging, Vib. Spectrosc., 48, 22–27, 2008.

Dieing, T., Hollricher, O., and Toporski, J.: Confocal raman microscopy, 1st ed., Springer series in optical sciences, Springer, 290 pp., 2011.

Finch, A. A. and Allison, N.: Mg structural state in coral aragonite and implications for the paleoenvironmental proxy, Geophys. Res. Lett., 35, L08704, doi:10.1029/2008gl033543, 2008.

Gautret, P., Cuif, J.-P., and Stolarski, J.: Organic components of the skeleton of scleractinian corals – evidence from *in situ* acridine orange staining, Acta Palaeontol. Pol., 45, 107–118, 2000.

Goreau, T. F.: The physiology of skeleton formation in corals, I. A method for measuring the rate of calcium deposition by corals under different conditions, Biol. Bull., 116, 59–75, 1959.

Hild, S., Marti, O., and Ziegler, A.: Spatial distribution of calcite and amorphous calcium carbonate in the cuticle of the terrestrial crustaceans *Porcellio scaber* and *Armadillidium vulgare*, J. Strut. Biol., 163, 100–108, doi:10.1016/j.jsb.2008.04.010, 2008.

Houlbreque, F., Meibom, A., Cuif, J. P., Stolarski, J., Marrocchi, Y., Ferrier-Pages, C., Domart-Coulon, I., and Dunbar, R. B.: Strontium-86 labeling experiments show spatially heterogeneous skeletal formation in the scleractinian coral *Porites porites*, Geophys. Res. Lett., 36, L04604, doi:10.1029/2008gl036782, 2009.

Jolivet, A., Bardeau, J. F., Fablet, R., Paulet, Y. M., and de Pontual, H.: Understanding otolith biomineralization processes: new insights into microscale spatial distribution of organic and mineral fractions from Raman microspectrometry, Anal. Bioanal. Chem., 392, 551–560, doi:10.1007/s00216-008-2273-8, 2008.

Juillet-Leclerc, A., Reynaud, S., Rollion-Bard, C., Cuif, J. P., Dauphin, Y., Blamart, D., Ferrier-Pages, C., and Allemand, D.: Oxygen isotopic signature of the skeletal microstructures in cultured corals: Identification of vital effects, Geochim. Cosmochim. Ac., 73, 5320–5332, doi:10.1016/j.gca.2009.05.068, 2009.

Kaczorowska, B., Hacura, A., Kupka, T., Wrzalik, R., Talik, E., Pasterny, G., and Matuszewska, A.: Spectroscopic characterization of natural corals, Anal. Bioanal. Chem., 377, 1032–1037, doi:10.1007/s00216-003-2153-1, 2003.

Lough, J. M. and Barnes, D. J.: Environmental controls on growth of the masisve coral *Porites*, J. Exp. Mar. Biol. Ecol., 245, 225–243, 2000.

Meibom, A., Stage, M., Wooden, J., Constantz, B. R., Dunbar, R. B., Owen, A., Grumet, N., Bacon, C. R., and Chamberlain, C. P.: Monthly Strontium/Calcium oscillations in symbiotic coral aragonite: Biological effects limiting the precision of the paleotemperature proxy, Geophys. Res. Lett., 30, 1418, doi:10.1029/2002gl016864, 2003.

Meibom, A., Cuif, J. P., Hillion, F. O., Constantz, B. R., Juillet-Leclerc, A., Dauphin, Y., Watanabe, T., and Dunbar, R. B.: Distribution of magnesium in coral skeleton, Geophys. Res. Lett., 31, L23306, doi:10.1029/2004gl021313, 2004.

Meibom, A., Mostefaoui, S., Cuif, J.-P., Dauphin, Y., Houlbreque, F., Dunbar, R., and Constantz, B.: Biological forcing controls the chemistry of reef-building coral skeleton, Geophys. Res. Lett., 34, L02601, doi:10.1029/2006GL028657, 2007.

Meibom, A., Cuif, J.-P., Houlbreque, F., Mostefaoui, S., Dauphin, Y., Meibom, K. L., and Dunbar, R.: Compositional variations at ultra-structure length scales in coral skeleton, Geochim. Cosmochim. Ac., 72, 1555–1569, 2008.

Milne-Edwards, H. and Haime, J.: Histoire naturelle des coralliaires ou polypes proprement dits, Tome 2: Classification et description des zoanthaires sclerodermes de la section des madréporaires apores, Paris, Librairie Ecyclopédique Roret, 633 pp., 1857.

Nehrke, G. and Nouet, J.: Confocal Raman microscope mapping as a tool to describe different mineral and organic phases at high spatial resolution within marine biogenic carbonates: case study on Nerita undata (Gastropoda, Neritopsina), Biogeosciences, 8, 3761–3769, doi:10.5194/bg-8-3761-2011, 2011.

Nehrke, G., Poigner, H., Wilhelms-Dick, D., Brey, T., and Abele, D.: Coexistence of three calcium carbonate polymorphs in the shell of the Antarctic clam Laternula elliptica, Geochem. Geophy. Geosy., 13, Q05014, doi:10.1029/2011gc003996, 2012.

Neues, F., Hild, S., Epple, M., Marti, O., and Ziegler, A.: Amorphous and crystalline calcium carbonate distribution in the tergite cuticle of moulting *Porcellio scaber* (Isopoda, Crustacea), J. Strut. Biol., 175, 10–20, doi:10.1016/j.jsb.2011.03.019, 2011.

Nothdurft, L. D. and Webb, G. E.: Microstructure of common reef-building coral genera *Acropora*, *Pocillopora*, *Goniastrea* and *Porites*: constraints on spatial resolution in geochemical sampling, Facies, 53, 1–26, 2007.

Ogilvie, M.: Microscopic and systematic study of Madreporarian types of corals, Philos. T. R. Soc. Lond., 187, 83–187, 1896.

Perrin, C. and Smith, D. C.: Earliest steps of diagenesis in living scleractinian corals: evidence from ultrastructural pattern and Raman spectroscopy, J. Sediment. Res., 77, 495–507, 2007.

Pratz, E.: Über die verwandtschaftlichen Beziehungen einiger Korallengattungen mit hauptsächlicher Berücksichtigung ihrer Septalstruktur, Palaeontographica, 29, 81–122, 1882.

Rollion-Bard, C., Chaussidon, M., and France-Lanord, C.: pH control on oxygen isotopic composition of symbiotic corals, Earth Planet. Sc. Lett., 215, 275–288, 2003.

Rollion-Bard, C., Blamart, D., Cuif, J. P., and Dauphin, Y.: In situ measurements of oxygen isotopic composition in deep-sea coral, *Lophelia pertusa*: Re-examination of the current geochemical models of biomineralization, Geochim. Cosmochim. Ac., 74, 1338–1349, doi:10.1016/j.gca.2009.11.011, 2010.

Smith, E. and Dent, G.: Modern Raman spectroscopy – a practical approach, West Sussex, UK, John Wiley & Sons Ltd., 210 pp., 2005.

Sorauf, J.: Skeletal microstructure and microarchitecture in scleractinian (Coelenterata), Palaeontology, 15, 88–107, 1972.

Sorauf, J. and Jell, J. S.: Strucutre and incremental growth in the ahermatypic coral *Desmophyllum cristagalli* from the north Atlantic, Palaeontology, 20, 1–19, 1977.

Stolarski, J.: Three-dimensional micro- and nanostructural characteristics of scleractinian coral skeleton: A biocalcification proxy, Acta Palaeontol. Pol., 48, 497–530, 2003.

Thebault, J., Chauvaud, L., Clavier, J., Fichez, R., and Morize, E.: Evidence of a 2-day periodicity of striae formation in the tropical scallop *Comptopallium radula* using calcein marking, Mar. Biol., 149, 257–267, doi:10.1007/s00227-005-0198-8, 2006.

Urmos, J., Sharma, S. K., and Mackenzie, F. T.: Characterization of some biogenic carbonates with Raman-spectroscopy, Am. Mineral., 76, 641–646, 1991.

Veron, J. E. N.: Corals of the World, Volume 1, Australian Institute of Marine Science, Townsville, 2000.

von Heider, A. R.: Korallenstudien, Zeitsch. der Wissensch. Zool., 46, 507–535, 1886.

von Koch, G.: Über das Verhältniss von Skelett und Weichtheilen bei den Madreporaren, Morph. Jahrb. 12, 154–162, 1887.

Waite, J. and Andersen, O.: 3,4-dihydroxyphenylalanine (DOPA) and sclerotization of periostracum in *Mytilus edulis* l., Biol. Bull., 158, 164–173, 1980.

Zhang, F., Cai, W., Sun, Z., and Zhang, J.: Regular variations in organic matrix composition of small yellow croaker (*Pseudociaena polyactis*) otoliths: an in situ Raman microspectroscopy and mapping study, Anal. Bioanal. Chem., 390, 777–782, doi:10.1007/s00216-007-1695-z, 2008.

Zhang, F. F., Cai, W. Y., Zhu, J. C., Sun, Z. R., and Zhang, J.: In Situ Raman Spectral Mapping Study on the Microscale Fibers in Blue Coral (*Heliopora coerulea*) Skeletons, Anal. Chem., 83, 7870–7875, doi:10.1021/ac2017663, 2011.